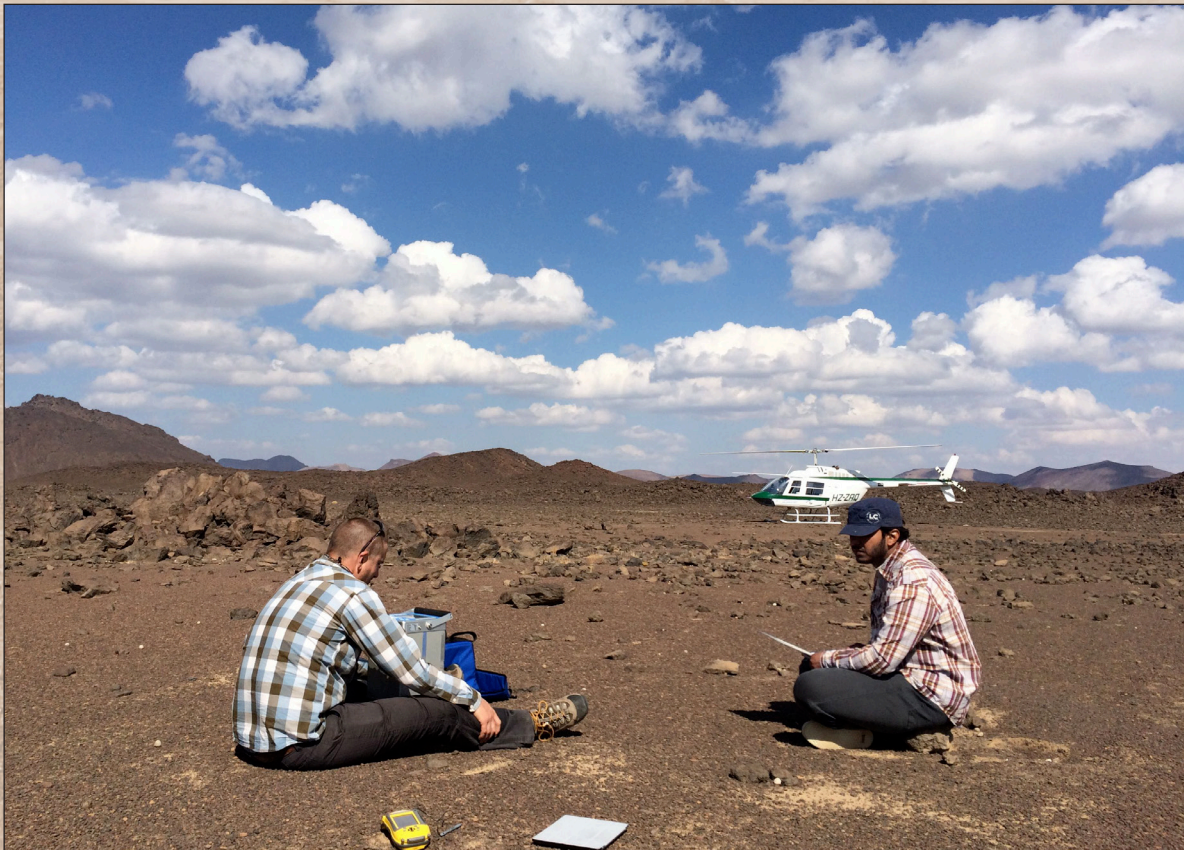


Depth to Basement and Crustal Structure of the Northern Harrat Rahat Volcanic Field, Kingdom of Saudi Arabia, from Gravity and Aeromagnetic Data

Chapter K of

Active Volcanism on the Arabian Shield—Geology, Volcanology, and Geophysics of Northern Harrat Rahat and Vicinity, Kingdom of Saudi Arabia



U.S. Geological Survey Professional Paper 1862
Saudi Geological Survey Special Report SGS–SP–2021–1

Cover. Photograph of authors Brent Ritzinger (left) and Maher Al-Dhahry (right) making a gravity measurement in the field. U.S. Geological Survey photograph by Victoria Langenheim, November 2014. Background image shows northern Harrat Rahat lava flows, maars, and lava domes. U.S. Geological Survey photograph by Andrew Calvert, January 25, 2012.

Depth to Basement and Crustal Structure of the Northern Harrat Rahat Volcanic Field, Kingdom of Saudi Arabia, from Gravity and Aeromagnetic Data

By Victoria E. Langenheim, Brent T. Ritzinger, Hani M. Zahran, Adel Shareef, and Maher K. Al-Dhahry

Chapter K of

Active Volcanism on the Arabian Shield—Geology, Volcanology, and Geophysics of Northern Harrat Rahat and Vicinity, Kingdom of Saudi Arabia

Edited by Thomas W. Sisson, Andrew T. Calvert, and Walter D. Mooney

U.S. Geological Survey Professional Paper 1862
Saudi Geological Survey Special Report SGS–SP–2021–1

U.S. Department of the Interior
U.S. Geological Survey

U.S. Geological Survey, Reston, Virginia: 2023

For more information on the USGS—the Federal source for science about the Earth, its natural and living resources, natural hazards, and the environment—visit <https://www.usgs.gov> or call 1-888-ASK-USGS.

For an overview of USGS information products, including maps, imagery, and publications, visit <https://store.usgs.gov>.

Any use of trade, firm, or product names is for descriptive purposes only and does not imply endorsement by the U.S. Government.

Although this information product, for the most part, is in the public domain, it also may contain copyrighted materials as noted in the text. Permission to reproduce copyrighted items must be secured from the copyright owner.

Suggested citation:

Langenheim, V.E., Ritzinger, B.T., Zahran, H.M., Shareef, A., and Al-Dhahry, M.K., 2023, Depth to basement and crustal structure of the northern Harrat Rahat volcanic field, Kingdom of Saudi Arabia, from gravity and aeromagnetic data, chap. K of Sisson, T.W., Calvert, A.T., and Mooney, W.D., eds., Active volcanism on the Arabian Shield—Geology, volcanology, and geophysics of northern Harrat Rahat and vicinity, Kingdom of Saudi Arabia: U.S. Geological Survey Professional Paper 1862 [also released as Saudi Geological Survey Special Report SGS-SP-2021-1], 18 p., <https://doi.org/10.3133/pp1862K>.

Associated data for this publication:

Langenheim, V.E., 2018, Gravity and physical property data of the northern Harrat Rahat, Saudi Arabia: U.S. Geological Survey data release, <https://doi.org/10.5066/P9THCSE8>.

ISSN 1044-9612 (print)
ISSN 2330-7102 (online)



هيئة المساحة الجيولوجية السعودية
SAUDI GEOLOGICAL SURVEY

Ministry of Industry and Mineral Resources

BANDAR BIN IBRAHIM BIN ABDULLAH AL-KHORAYEF, Minister and SGS Chairman

Saudi Geological Survey

Abdullah bin Mufter Al-Shamrani, Chief Executive Officer

Saudi Geological Survey, Jiddah, Kingdom of Saudi Arabia: 2023

Contents

| | |
|-----------------------------------|----|
| Abstract..... | 1 |
| Introduction..... | 1 |
| Geology..... | 2 |
| Geophysical Data..... | 4 |
| Geophysical Anomalies | 5 |
| Modeling of Data..... | 8 |
| Depth to Basement Inversion | 8 |
| 2D Modeling..... | 10 |
| Discussion..... | 13 |
| Conclusions..... | 15 |
| Acknowledgments..... | 15 |
| References Cited..... | 16 |

Figures

| | |
|--|----|
| 1. Plate tectonic setting of Cenozoic volcanic fields within the Arabia Plate | 2 |
| 2. Geologic map of northern Harrat Rahat and surrounding area..... | 3 |
| 3. Complete Bouguer gravity map..... | 4 |
| 4. Reduced-to-pole aeromagnetic maps and anomalies | 6 |
| 5. Map showing distribution of samples used to determine bulk rock densities and histogram showing distribution of rock densities | 7 |
| 6. Map of depth to basement and basement gravity field | 9 |
| 7. Forward gravity models of profile <i>A–A'</i> | 11 |
| 8. Forward gravity models of profile <i>E–E'</i> | 12 |
| 9. Plot of topography and basement surfaces across Harrat Rahat..... | 14 |
| 10. Map of the elevation of basement surface. Black lines, modeled cross sections..... | 15 |

Conversion Factors

International System of Units to U.S. customary units

| Multiply | By | To obtain |
|---|---------|--|
| Length | | |
| meter (m) | 3.281 | foot (ft) |
| kilometer (km) | 0.6214 | mile (mi) |
| kilometer (km) | 0.5400 | mile, nautical (nmi) |
| meter (m) | 1.094 | yard (yd) |
| Flow rate | | |
| kilometer per second (km/s) | 0.6214 | mile per second (mi/s) |
| Density | | |
| kilogram per cubic meter (kg/m ³) | 0.06242 | pound per cubic foot (lb/ft ³) |

Temperature in degrees Celsius (°C) may be converted to degrees Fahrenheit (°F) as follows:

$$^{\circ}\text{F} = (1.8 \times ^{\circ}\text{C}) + 32.$$

Abbreviations

| | |
|-----------|--|
| 2D | two dimensional |
| 3D | three dimensional |
| C.E. | Common Era |
| GPS | Global Positioning System |
| lidar | light detection and ranging |
| Ma | million years ago |
| mGal | milligal |
| μGal | microgal |
| Moho | Mohorovičić discontinuity |
| V_p/V_s | ratio of seismic P-wave to S-wave velocity |

Chapter K

Depth to Basement and Crustal Structure of the Northern Harrat Rahat Volcanic Field, Kingdom of Saudi Arabia, from Gravity and Aeromagnetic Data

By Victoria E. Langenheim,¹ Brent T. Ritzinger,¹ Hani M. Zahran,² Adel Shareef,² and Maher K. Al-Dhahry²

Abstract

New gravity data reveal a prominent negative anomaly along the main vent axis of the northern Harrat Rahat volcanic field in the Kingdom of Saudi Arabia. The gravity low continues north of the volcanic field onto exposures of Proterozoic rocks, indicating that the low is caused not only by the volcanic field (and possibly underlying Cenozoic sediments), but also the underlying Proterozoic basement. An inversion of the gravity field guided by analysis of aeromagnetic data indicates (1) a broad depression of the basement surface that is deeper along the main vent axis in the eastern part and in the southwest part of the volcanic field and (2) less dense basement beneath the vent axis. Low densities within the basement most likely arise from lithologic variations in the basement, predating Cenozoic volcanism, although our analysis does not rule out small volumes of partial melt and higher temperatures or extensive fracturing at depth.

Introduction

Cenozoic volcanic fields along the western margin of the Arabia Plate (fig. 1) have been attributed to asthenospheric upwelling (Camp and Roobol, 1992), as evidenced by slower seismic velocities in the mantle (Rodgers and others, 1999). How this deep mantle structure relates to the plumbing and crustal structure of these volcanic fields (“harrats” in Arabic) is only recently being addressed (for example, Abdelwahed and others, 2016), motivated by an unusually energetic earthquake swarm in 2009 caused by a dike intrusion beneath Harrat Lunayyir (Pallister and others, 2010). Of particular interest is Harrat Rahat, one of the largest volcanic fields in the Kingdom of Saudi Arabia (Coleman and others, 1983; Camp and Roobol, 1989), which produced lava flows in 1256 C.E. that came within 8 kilometers of the center of the holy city of Al Madīnah al Munawwarah (Camp and others, 1987).

The harrats in Saudi Arabia overlie Neoproterozoic crust of the Arabian Shield, which is an assemblage of arc terranes bounded by ophiolite-lined sutures (Stern and Johnson, 2010).

The degree to which these ancient shield structures influence harrat volcanism is much debated. Seismic anisotropy indicates a north-south fabric in the mantle beneath central Arabia, which has been interpreted as fossil lithospheric shear zones developed during Neoproterozoic collision (Levin and Park, 2000) or as the vector sum of northwest channelized asthenospheric flow and northeast motion of the Arabia Plate (Hansen and others, 2006). Camp and Roobol (1989) mapped geomorphic lineaments within Harrat Rahat inferred to be reactivation along Proterozoic northwest-, northeast-, and east-west-trending faults. They noted, however, the lack of exposed deformational features, such as fault gouge or slickensides and recently more detailed topography and field observations fail to support these lineaments as structural features (Downs and others, 2019; Robinson and Downs, 2023). Phanerozoic reactivation of Proterozoic structure is plausible, but such evidence is difficult to document in the Arabian Shield because of the near absence of suitably aged deposits (Stern and Johnson, 2010). A more complete three-dimensional (3D) crustal framework would help address the influence of older structures on Cenozoic deformation and volcanism.

In a few places, Cenozoic volcanic rocks are underlain by marls and gravels, interpreted as having been deposited in a wide zone of crustal extension in the early stages of Red Sea rifting during the early Miocene (Coleman and others, 1983; Coleman, 1993), which suggests that the volcanic fields are underlain by basins or grabens. Identifying basins and bounding faults concealed beneath the harrats is important for assessing seismic hazard. Two previous studies show significantly different basement surfaces beneath northern Harrat Rahat: a subvolcanic basement surface no deeper than 500 meters (m) above sea level as “revealed by geophysics” (Daesslé and Durozoy, 1972, in figure 2 of Pellaton, 1981), versus a basement surface deeper than 600 m below sea level as derived from analysis of gridded aeromagnetic data (Aboud and others, 2015).

This chapter adapts much of what was published by Langenheim and others (2019). That paper used gravity data to determine crustal structure and identify significant faults beneath northern Harrat Rahat. In particular, an inversion of gravity data explicitly uses geologic constraints to estimate the depth to Proterozoic basement and map significant faults

¹U.S. Geological Survey.

²Saudi Geological Survey

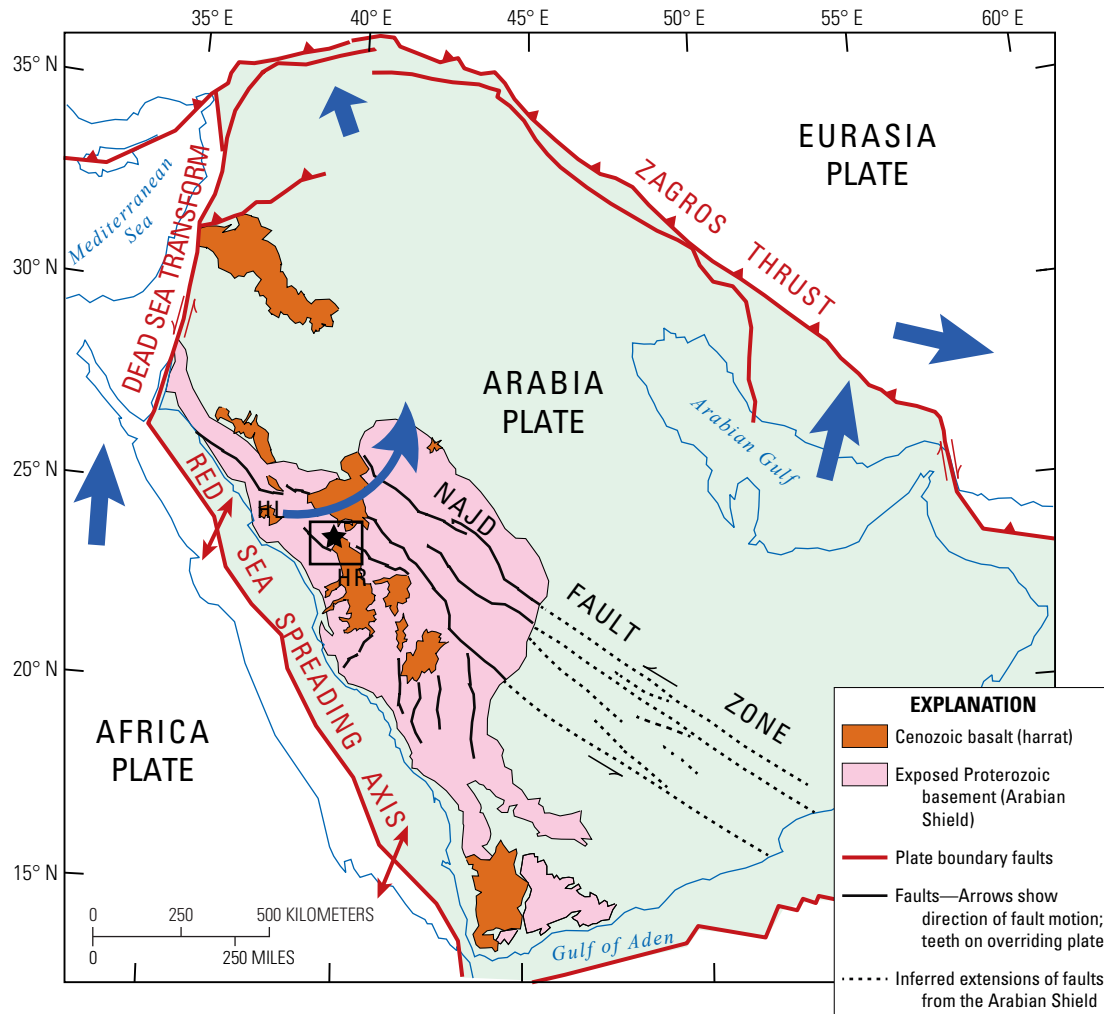


Figure 1. Plate tectonic setting of Cenozoic volcanic fields within the Arabia Plate (modified slightly from Stern and Johnson, 2010). Blue arrows denote plate motions. Star marks location of Al Madinah. HL, Harrat Lunayyir; HR, Harrat Rahat. Black box shows study area.

concealed beneath the young volcanic cover. Langenheim and others (2019) also combined analysis of the gravity data with existing aeromagnetic data to examine Proterozoic basement structure and its possible influence on the plumbing of the Harrat Rahat volcanic field, and modification of the Proterozoic crust by Cenozoic volcanism.

Geology

Cenozoic volcanic rocks of northern Harrat Rahat (fig. 2) lap onto and overlie Proterozoic rocks of the Hijaz terrane, which is composed of volcanic arc rocks and younger volcanic sedimentary successions. In the study area, the Al Ays and Birak Groups of the Hijaz terrane, predominantly mafic to silicic volcanic rocks and derivative epiclastic sedimentary rocks, are overlain unconformably by the sedimentary and volcanic sequence of the Furayh Group (Pellaton, 1981; Camp, 1986). Granite and granodiorite intrusions predate and postdate deposition of the Furayh Group. Diorite and gabbro form smaller stocks. Dike swarms

intrude all of the Proterozoic units (except for the peralkalic granite in the southwest part of the study area) and are most prevalent west of Harrat Rahat (Pellaton, 1981; Camp, 1986). The Proterozoic rocks have been regionally metamorphosed to greenschist facies.

Metamorphism was accompanied by folding. North-northeast- to north-northwest-trending folds deform the volcanic-sedimentary groups. Older rocks are folded more intensely than younger rocks (Camp, 1986), suggesting at least two episodes of deformation. Of particular interest is the syncline ~15 kilometers (km) northeast of Al Madinah, representing a major phase of folding that also affected monzonite and gabbro intrusions north of the map area (Pellaton, 1981). South of the study area, fold axes trend north to north-northeast, but curve to a northwest orientation in proximity to the Najd Fault (fig. 2; Camp, 1986), a strand of a major sinistral fault system that strikes N. 40°–50° W. and extends across the Arabian Shield (fig. 1). Another strand of this fault system northwest of the city of Al Madinah offsets a pluton by as much as 8 km (Pellaton, 1981; labeled “P” in fig. 2).

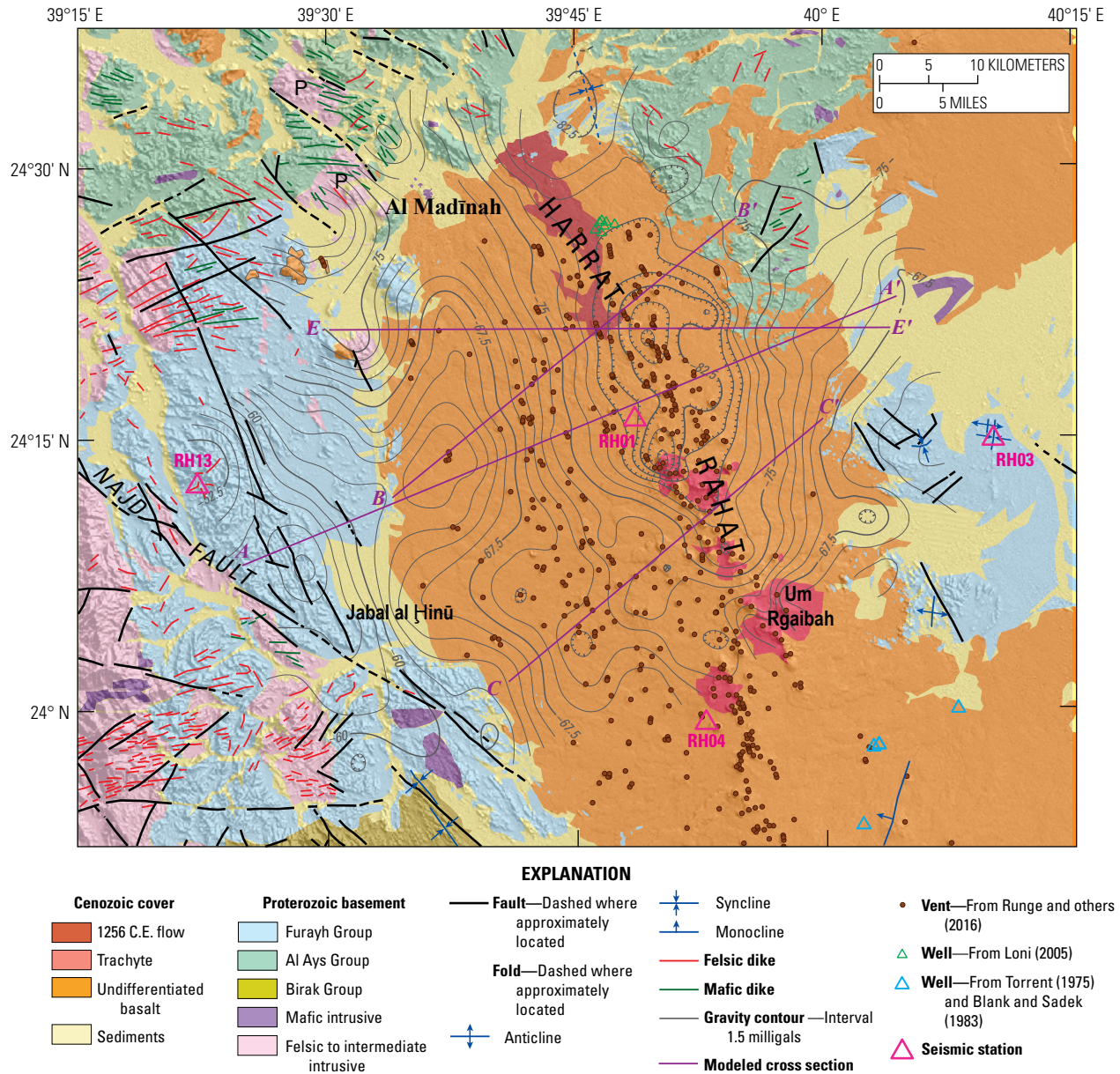


Figure 2. Geologic map of northern Harrat Rahat and surrounding area, simplified from Pellaton (1981) and Camp (1986), north and south of latitude 24° N., respectively. Vents from Runge and others (2016); wells from Loni (2005; green triangles ~10 kilometers east of Al Madinah) and from Torrent (1975) and Blank and Sadek (1983; cyan triangles in southeast part of map area). Modeled cross sections shown in figures 7 (A–A’), 8 (E–E’), and 9 (B–B’, C–C’). P, plutons offset by a strand of the Najd Fault System.

Folding predated deposition of nearly horizontal Cambrian-Ordovician strata northeast of the map area, and the Najd Fault System ceased activity before the Cambrian. Just north of the map area, some strands of the Najd Fault System project toward a granite pluton dated to 561 million years ago (Ma) without offsetting it (Pellaton, 1981).

Volcanic rocks of Harrat Rahat overlie the complex Proterozoic basement. The north-trending volcanic field is predominantly mafic, covers ~20,000 square kilometers, and is more than 300 km long. The northern third of the Harrat Rahat, our study area, consists primarily of alkali basalt with minor

amounts of hawaiite, mugearite, benmoreite, and trachyte (Camp and Roobol, 1989; Stelten and others, 2018, 2023; Downs and others, 2019; Robinson and Downs, 2023). New age dates indicate that the volcanic field in the study area is almost entirely Pleistocene in age (Stelten and others, 2018, 2023; Downs and others, 2018, 2019), refining previous results of Camp and Roobol (1989) and Moufti and others (2013) that indicated volcanism extending into the Pliocene and Miocene. The trachytes, representing the most evolved lavas of the harrat, erupted from the southern part of the study area starting at about 150,000 years ago (Stelten and others, 2018, 2023).

4 Active Volcanism on the Arabian Shield—Geology, Volcanology, and Geophysics

Most of the vents that produced the lavas and small-volume pyroclastic flows of northern Harrat Rahat form a north-south alignment along the axis of the volcanic field (Runge and others, 2016). Analysis of vent density indicates that the highest density of vents is along the axis, with a secondary alignment ~10 km to the west (Dietterich and others, 2017). In the southern part of the study area, the vents appear to coalesce into a single alignment at about latitude 24° N. (fig. 2).

Geophysical Data

More than 300 gravity measurements were collected in northern Harrat Rahat in November and December 2014 with a spacing of 1–3 km between sites within the harrat and somewhat wider spacing outside the harrat (fig. 3); no other gravity measurements in the area are publicly available. Use of a helicopter facilitated access to the volcanic field and adjacent mountains. Scintrex CG5 gravity meters were used

to measure gravity values, which were then corrected for tidal variations and instrument drift and tied to the absolute gravity station AG0191 located on the Madinah Technical College campus (978,710.191 milligals [mGal], lat 24°28'52" N., long 39°42'56" E.). The instruments behaved well, with a maximum daily drift of 37 microgals (μGal) (average $12 \pm 9 \mu\text{Gal}$). To obtain accurate elevations of the gravity measurements, we used Trimble PathFinder Office software (www.geospatial.trimble.com) to process GPS (Global Positioning System) data obtained with a Trimble GeoXH receiver and using Saudi Geological Survey continuously operating GPS stations as reference points. The resulting elevations compared favorably (<0.3 m) with elevations from a lidar (light detection and ranging) survey, as well as 1-m and 4-m digital elevation models. We used GeoSoft Oasis Montaj software (www.geosoft.com) to calculate free-air, simple, and complete Bouguer gravity anomalies. Terrain corrections were obtained using terrain data from the Shuttle Radar Topography Mission and using a standard crustal reduction density of

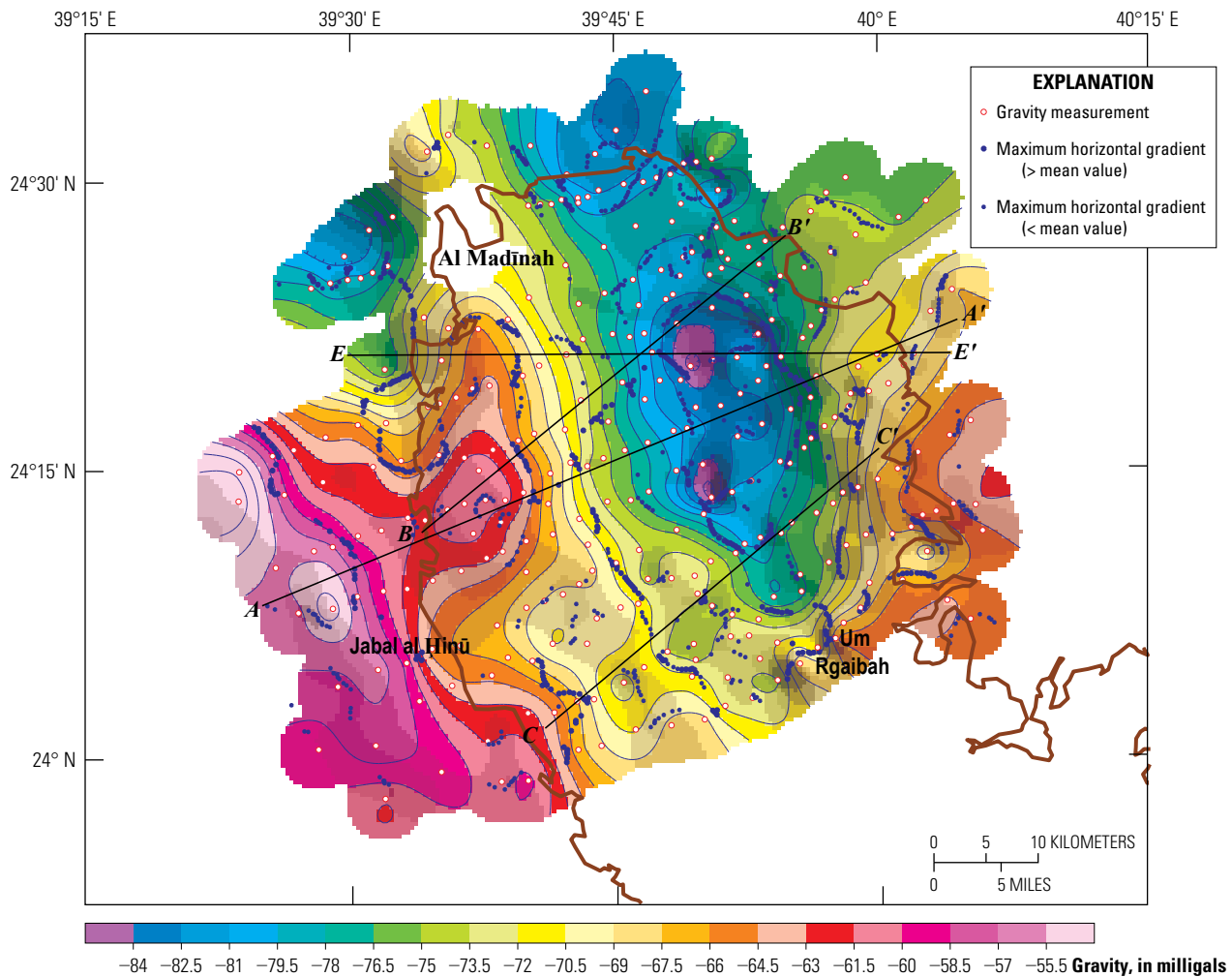


Figure 3. Complete Bouguer gravity map. Contour interval, 1.5 milligals (mGal). Red-rimmed white circles, gravity measurement sites. Dark blue dots, density boundaries from maximum horizontal gradient method. Larger gradients are more prominent. Black lines, modeled cross sections (see figs. 7–9). Brown line, extent of Harrat Rahat volcanic field.

2,670 kilograms per cubic meter (kg/m^3). The resulting gravity anomaly values are estimated to be accurate to <0.5 mGal, with most of the values accurate to <0.2 mGal. Bouguer gravity anomalies over volcanic terrain commonly exhibit topographic artifacts because the reduction density is higher than volcanic materials. This is not the case in our survey because of the generally subdued topography of Harrat Rahat, and because we purposely avoided measurements on top of volcanic cones and domes.

Aeromagnetic data are from the compilation of Zahran and others (2003) and include several surveys. Data east and west of Harrat Rahat were flown along flight lines spaced 800 m apart and at elevations of 150 and 300 m above terrain, respectively. Aeromagnetic data over Harrat Rahat consist of flight lines at a similar height above ground (300 and 500 m), but with significantly larger flight-line spacing (2,000 m north of lat 24° N. and 2,500 m south of lat 24° N.), resulting in a loss of detail and aliasing effects (Reid, 1980). Total-field anomalies were calculated by subtracting the International Geomagnetic Reference Field from total-field measurements.

The change in anomaly character caused by flight-line spacing is noticeable where higher resolution data extend across the volcanic field, with resulting short wavelength anomalies compared to smoother, longer wavelength anomalies revealed by the lower resolution surveys. The aeromagnetic anomalies in figure 4 have been reduced to pole, as discussed by Zahran and others (2003), thereby accounting for the inclination of the Earth's magnetic field. Figure 4B shows magnetic anomalies after application of a matched filter (Phillips, 2001) to emphasize wavelength components that equate to a source layer at ~ 7 km depth. Note that the actual source depth may be shallower, given that broader wavelength anomalies can be fit by both deep and shallow sources.

We used gradients of the gravity and magnetic fields to map locations of geologic contacts (figs. 3 and 4A). The method (Cordell and Grauch, 1985; Blakely and Simpson, 1986) exploits the fact that gravity anomalies and magnetic anomalies converted to magnetic potential (the equivalent "gravity" field if all magnetic material were replaced by proportionately dense material; Baranov, 1957) have steepest horizontal gradients directly over steeply dipping contacts.

Density and magnetic properties of rock samples are crucial parameters for analyzing and modeling gravity and magnetic data. Hand-sized or larger samples of Harrat Rahat volcanic rocks ($N=527$) collected by U.S. Geological Survey geologists for petrography, geochemistry, and geochronology were measured for density (fig. 5) and magnetic susceptibility (not shown; Langenheim, 2018). These samples are generally from the freshest and densest parts of the volcanic sequence. Samples of Proterozoic formations ($N=54$) were also collected, where feasible. Densities were determined using a precision Sartorius electronic balance. All rocks were weighed dry in air (W_a), saturated in water (W_w), and saturated with water in air (W_s). From these measurements, grain density,

dry-bulk density, and saturated-bulk density were calculated using the following formulas.

$$\text{Grain density} = (\rho_w \times W_a) / (W_a - W_w),$$

$$\text{Dry bulk density} = (\rho_w \times W_a) / (W_s - W_w), \text{ and}$$

$$\text{Saturated bulk density} = (\rho_w \times W_s) / (W_s - W_w),$$

where ρ_w is the density of water ($1,000 \text{ kg/m}^3$).

Magnetic susceptibilities were measured with a Geophysica KT-5 susceptibility meter and are reported to an accuracy of 0.1 to 0.01×10^{-3} SI units. The Geophysica KT-5 calculates volume susceptibility by assuming the sample shape is an infinite half-space. The instrument's ability to measure magnetic susceptibility is affected by surface roughness, weathering, and sample size, all of which can result in an underestimation of a sample's true susceptibility. The magnetic-susceptibility values reported represent the highest reading on the hand sample. Note these values do not take into account remanent magnetization, which is an important component of the total magnetization, particularly for the mainly Quaternary volcanic rocks of Harrat Rahat.

Geophysical Anomalies

The new gravity data (figs. 2 and 3) reveal a prominent, north-northwest-trending gravity low that extends about 30 km north of Um Rgaibah approximately along the main topographic axis of the volcanic field and along the main alignment of volcanic vents. Gravity highs occur over Proterozoic basement to the southwest, east, and locally to the north, suggesting that the source of the gravity low results from density contrasts between low-density rocks composed of harrat volcanic rocks and potential basin deposits beneath the harrat and the underlying higher density Proterozoic basement. Although the densities of the volcanic rocks are highly variable (fig. 5), they are on average less dense than the Proterozoic basement and must contribute to the gravity low over the axis of the northern Harrat Rahat.

The western margin of the low is marked by a significant north- to north-northwest-trending gravity gradient that bisects the volcanic field (fig. 2). A steeper, north-trending gravity gradient defines the eastern edge of the gravity low, about 1–2 km west of outcrops of the Furayh Group (fig. 2), and extending for 15–20 km north-south, as far north as the latitude of profile $E-E'$. North of profile $E-E'$, the gradient becomes more diffuse and has a north-northwesterly trend. The gravity low narrows to the south where it steps 5 km westward and has significantly lower amplitude around a northeast-trending gravity high at Um Rgaibah. The gravity low at the northern end of the volcanic field continues north past a slight saddle east of Al Madīnah onto outcrops of Proterozoic basement.

6 Active Volcanism on the Arabian Shield—Geology, Volcanology, and Geophysics

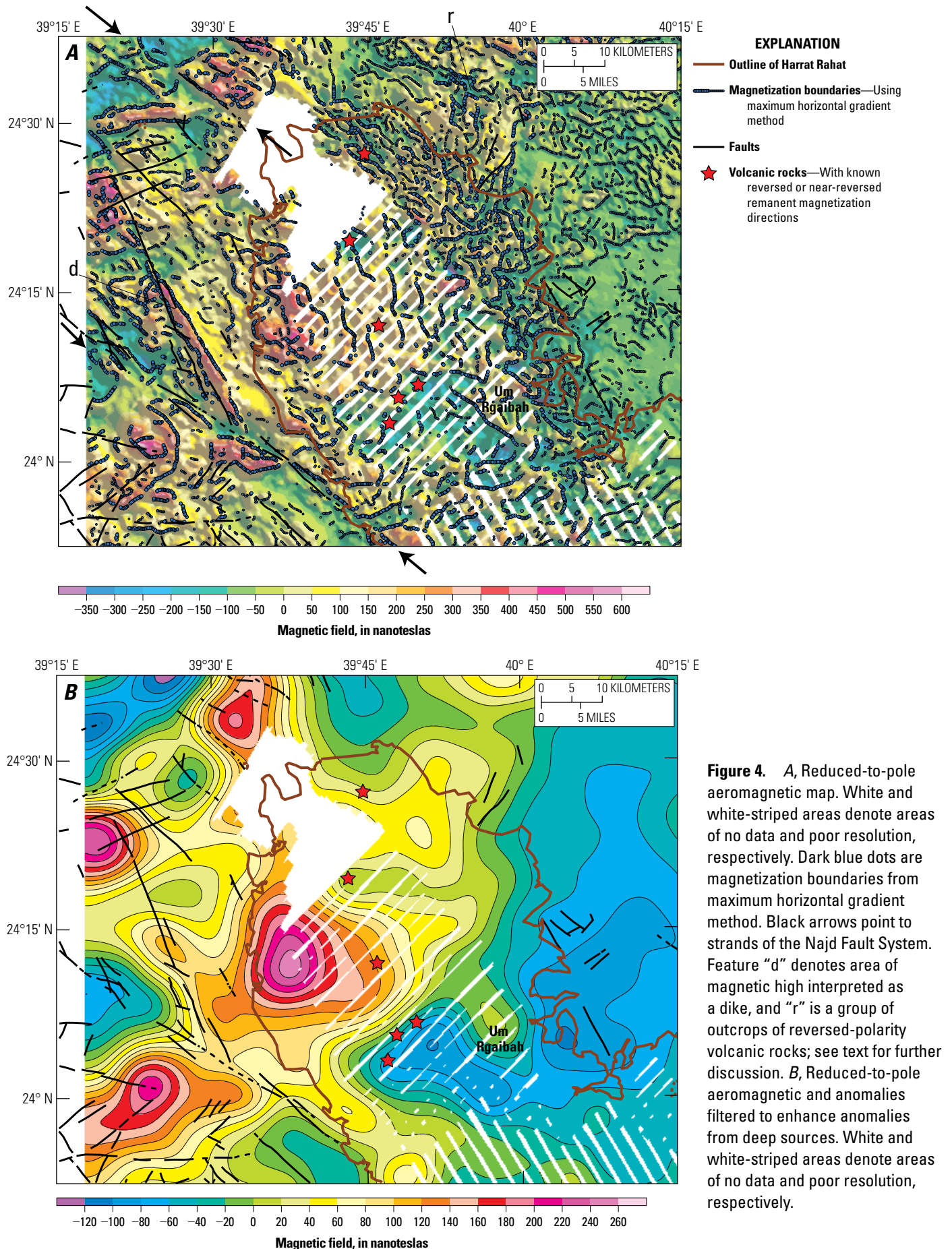


Figure 4. *A*, Reduced-to-pole aeromagnetic map. White and white-striped areas denote areas of no data and poor resolution, respectively. Dark blue dots are magnetization boundaries from maximum horizontal gradient method. Black arrows point to strands of the Najd Fault System. Feature “d” denotes area of magnetic high interpreted as a dike, and “r” is a group of outcrops of reversed-polarity volcanic rocks; see text for further discussion. *B*, Reduced-to-pole aeromagnetic and anomalies filtered to enhance anomalies from deep sources. White and white-striped areas denote areas of no data and poor resolution, respectively.

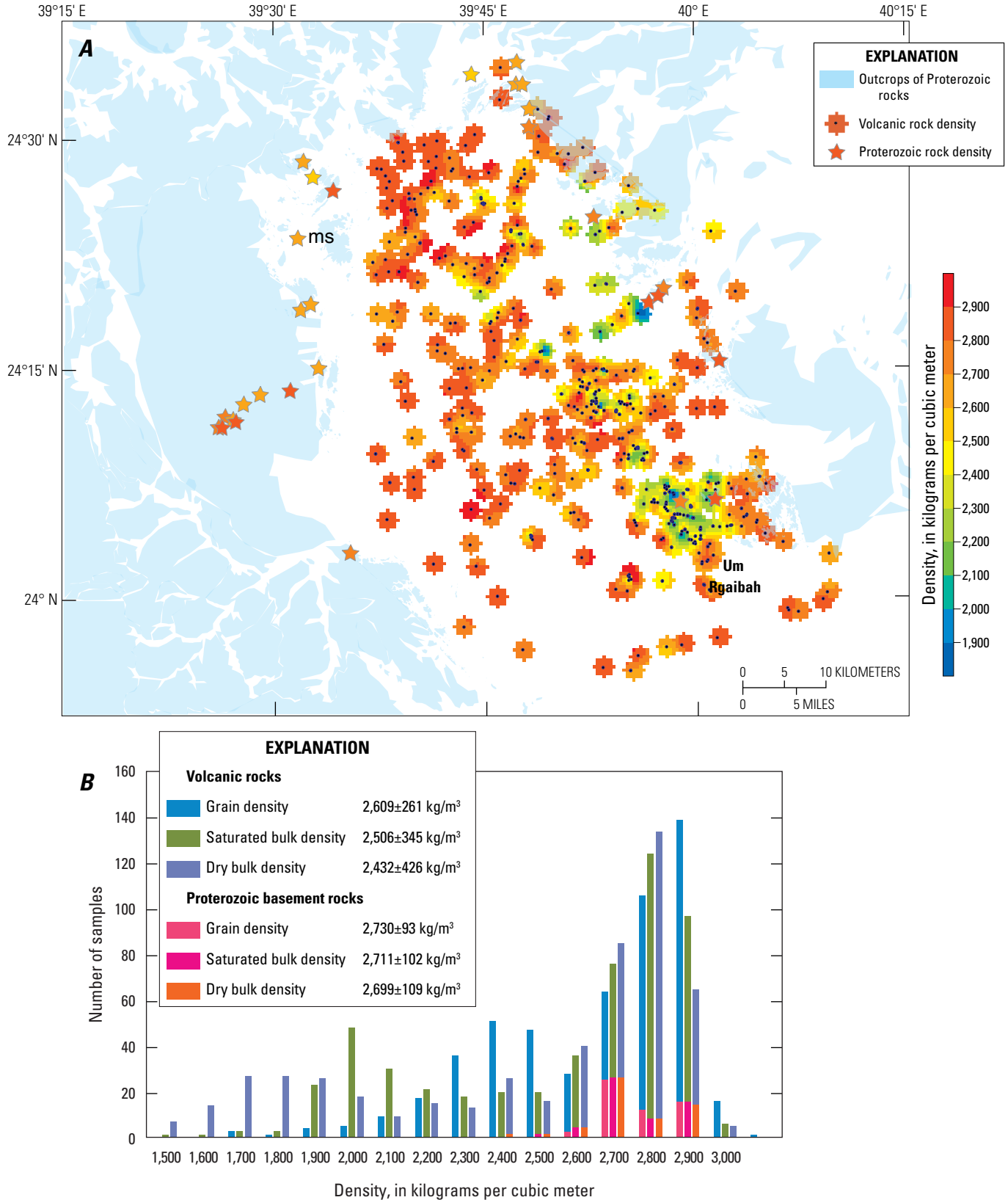


Figure 5. A, Map showing distribution of samples used to determine bulk rock densities, color coded by density. Cenozoic volcanic rocks, eight-pointed stars; Proterozoic rocks, five-pointed stars. Blue polygons, outcrops of Proterozoic rocks. Star labeled “ms,” mudstone locality discussed in text. B, Histogram showing distribution of rock densities (N=527) and Proterozoic basement rock (N=54) densities. Average densities (± 1 standard deviation) are given. kg/m³, kilograms per cubic meter.

The western part of the volcanic field coincides with a pear-shaped gravity high elongated in a north-south direction and reaching values that locally exceed those measured on Proterozoic basement. The gravity high extends north through the city of Al Madīnah onto basement outcrops. A gravity low lies west of the pear-shaped high and the city of Al Madīnah. The gravity low, defined by gravity measurements made on basement to the south, north, and east of the low, has an amplitude similar to the low east of the city.

These observations indicate that the prominent gravity low is not simply caused by lower density volcanic and sedimentary rocks, but is also caused by sources beneath the volcanic field within the basement. We rule out crustal thickness variations to account for the gravity anomalies because the Mohorovičić discontinuity (Moho) across the area appears to be fairly flat at a depth of about 35 km (Tang and others, 2016) and because such a deep source would produce gentler gravity gradients than are observed. Possible sources for the gravity low include density variations within the Proterozoic basement or crustal alteration by volcanic processes, such as intrusions or partial melt, as inferred by Abdelwahed and others (2016) based on P-wave tomography and by Aboud and others (2018) using magnetotelluric data.

The aeromagnetic data (fig. 4A) provide additional information on crustal structure, thus complementing the gravity data and providing information over a larger area than covered by our gravity survey. Short-wavelength anomalies characterize areas of Cenozoic volcanic rocks, except in the central part of the volcanic field, where lower resolution data (marked by white strips in fig. 4A) lead to aliased, longer wavelength, smoother anomalies. Even so, where controlled by flight line data, magnetic lows coincide with known rocks of reversed or transitional polarity (stars in fig. 4A; Downs and others, 2018, 2019; Robinson and Downs, 2023). Correspondence of narrow, short-wavelength magnetic lows northeast of Harrat Rahat with mapped reversely magnetized volcanic rocks (marked “r” in fig. 4A) suggests that these rocks were erupted during a reversed-polarity epoch. Within Harrat Rahat, it is tempting to assign the generally low magnetic values west and south of Um Rgaibah (fig. 4A) to a thick sequence of reversed-polarity flows, but magnetic data filtered to enhance deep sources (fig. 4B) suggests that an alternative likely source is weakly magnetic Proterozoic basement. Similarly, higher magnetic values over the western part of Harrat Rahat may indicate flows of dominantly normal polarity, but the equivalent high in the filtered magnetic data (fig. 4B) and a corresponding gravity high suggest a magnetic source within the basement.

West of Harrat Rahat, the magnetic field is characterized by generally higher values than to the east, likely reflecting the presence of more Proterozoic or younger intrusive input and more mafic compositions in the Proterozoic volcanic arc sequences. One possible exception is a 30-km-long, narrow magnetic high in the western part of the study area (marked “d” in fig. 4A). The source of this linear anomaly does not crop out, but its western margin is bounded in most places by faults in

Proterozoic rocks. The source of anomaly “d” may not be limited to the study area because it appears to align with a similar set of narrow magnetic highs that can be traced nearly 800 km to the north and 200 km to the south. It is mostly parallel to a set of similarly narrow anomalies to the west that are attributed by Blank (1977) to dikes related to the early Miocene opening of the Red Sea. Thus the source of anomaly “d” could be a set of early Miocene dikes that were preferentially injected along favorably oriented fractures of Proterozoic faults.

Modeling of Data

The gravity and magnetic patterns described above indicate a variety of sources at different depths. Such a superposition of anomalies produced by various sources can result in interpretational ambiguities. The principal goals of a gravity study are to detect and quantify changes in mass at depth and to interpret the subsurface geologic structure.

We applied an inversion and two-dimensional (2D) models to isolate and interpret the sources of the gravity anomalies. Because gravity modeling is nonunique, we use geology, physical property measurements, and seismic velocity information to model the observed gravity anomalies to arrive at a geologically reasonable approximation of the density distribution that fit the data. We did not model the magnetic data because of their poor resolution across Harrat Rahat.

Depth to Basement Inversion

We used a 3D inversion of gravity anomalies to take advantage of the density contrast between denser Proterozoic basement and less dense Cenozoic volcanic and sedimentary deposits (referred to as “volcanic basin deposits”). The inversion method (Jachens and Moring, 1990) explicitly uses mapped geology as a first-order constraint and drill hole data and other geophysical data as additional constraints. The method separates the complete Bouguer gravity field (gridded using a 400-m cell size) into two components, the anomaly produced by variations in basement density and that caused by volcanic basin deposits. The latter component is then inverted for the thickness of basin deposits. The inversion method allows the density of basement to vary horizontally as needed, whereas the density of the basin-filling deposits is specified by a predetermined density-depth profile. The basement gravity field is first estimated by passing a surface through those values measured on basement outcrops using the minimum curvature algorithm (Briggs, 1974; Webring, 1981). This field is subtracted from the complete Bouguer gravity field to produce an initial estimate of the basin gravity. Because basement gravity values near the basin edge are affected by the gravity effect of the low-density volcanic basin fill and thus underestimated, a forward calculation of the basin gravity field is used to correct the basement gravity measurements. This process is repeated until further steps do not result in significant changes to the modeled thickness of the basin deposits, usually in five or six steps.

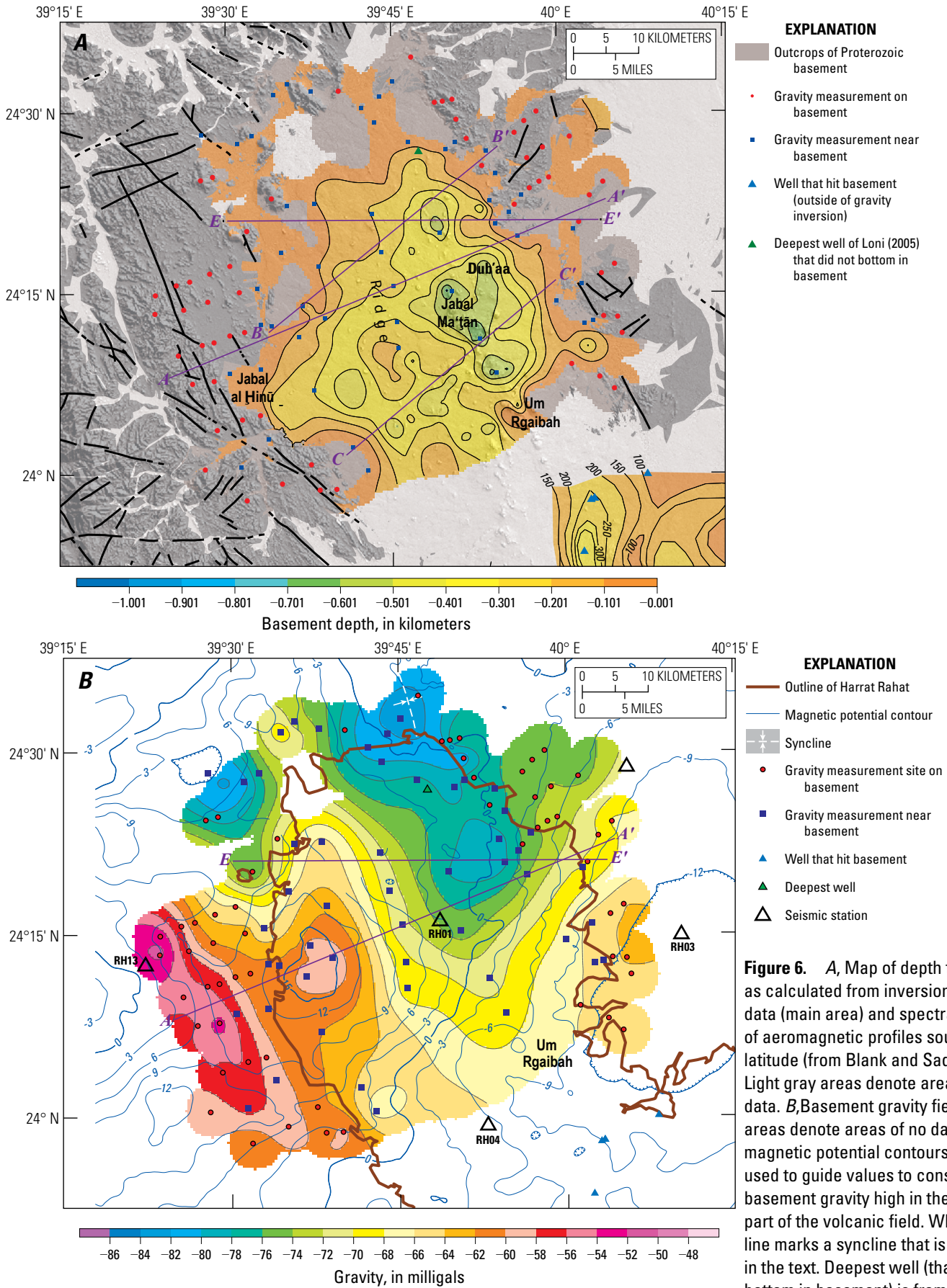


Figure 6. A, Map of depth to basement as calculated from inversion of gravity data (main area) and spectral analysis of aeromagnetic profiles south of 24° latitude (from Blank and Sadek, 1983). Light gray areas denote areas of no data. B, Basement gravity field. White areas denote areas of no data. The magnetic potential contours were used to guide values to constrain the basement gravity high in the western part of the volcanic field. White dashed line marks a syncline that is discussed in the text. Deepest well (that did not bottom in basement) is from Loni (2005).

We used a density contrast of -400 kg/m^3 to convert the basin gravity field to volcanic basin thickness (fig. 6A). This value is somewhat larger than the difference of the average volcanic density from the average Proterozoic density (fig. 5), but it is reasonable given the spread of values and sampling of the densest part of the volcanic flows for geochemistry and geochronology. Furthermore, our average density of Proterozoic basement ($\sim 2,710 \text{ kg/m}^3$) is somewhat lower than what would be predicted by seismic velocities of the upper 20 km from a refraction profile 500 km to the southeast (Mooney and others, 1985). Velocities of 6.1–6.4 kilometers per second (km/s) equate to densities of 2,733–2,845 kg/m^3 (Christensen and Mooney [1995] and Nafe-Drafe relation from Brocher [2005]). Such a density contrast seems reasonable, considering the average density of the Island of Hawai‘i (above sea level) is 2,300 kg/m^3 (Kauahikaua and others, 2000).

Of the few water wells with lithologic information available to us in northern Harrat Rahat, none penetrated basement within the area of the gravity survey (Loni, 2005). Thus, we used the deepest well (135 m) from Loni (2005) as a minimum constraint for the basement surface. We used the magnetic potential field contours (in fig. 6B) as a guide for basement gravity values over the prominent gravity high in the western part of Harrat Rahat. Highly magnetic rocks are commonly relatively dense. The magnetic potential field highlights voluminous magnetic sources, such as those lying beneath the volcanic field, and therefore should be a reasonable proxy for basement gravity variations. The northward decrease in basement gravity as measured on basement outcrops east of Harrat Rahat is also evident in the magnetic potential field, and so we used the magnetic potential data to extend that gradient across the volcanic field. The resulting basement gravity field (fig. 6B) shows a significant gravity low that extends south from Proterozoic basement outcrops, with gravity values gradually increasing southward, whereas a significant gravity high underlies the western part of Harrat Rahat, with gravity values gradually decreasing to the north. The basement gravity field also indicates a gravity low west of Al Madīnah, likely sourced by Proterozoic mudstone and siltstone of the Furayh Group, where densities range from 2,412 to 2,688 kg/m^3 (“ms” in fig. 5A).

The results of the inversion indicate that the thickest part of the volcanic basin fill lies roughly along the topographic axis of Harrat Rahat (fig. 6A), reaching values of 500–600 m, separated by a subtle ridge to the west underlying the central part of the volcanic field. The thicker volcanic rocks are bounded to the south by a ridge of very shallow basement near Um Rgaibah. This inference of a shallow basement is supported by the presence of abundant lithic clasts of Proterozoic basement that are part of the volcanic ejecta from this area, which differentiates this area from others in the northern Harrat Rahat (A. Calvert, oral commun., 2017). The inversion also suggests that shallow basement underlies the western part of Harrat Rahat, except near Jabal al Ḥinū, where the volcanic basin fill may be as much as 200–300 m thick. The modern drainage exits the mountains and flows

due north toward Al Madīnah, whereas the basin-fill thickness map (fig. 6A) suggests a paleodrainage concealed beneath the volcanic field that exits the mountain range west of the harrat and flows to the northeast before diverting around a concealed ridge. The average thickness of the volcanic basin fill over the area of Harrat Rahat in our study area is about 200 m.

2D Modeling

In addition to the 3D inversion, we used the Geosoft GM-SYS program (www.geosoft.com) to model two profiles that cross Harrat Rahat. The program requires an initial estimate of model parameters (depth, shape, and density of suspected sources). We used initial model estimates based on the shear-wave velocity model of Civilini (2018) and the P-wave tomography work of Abdelwahed and others (2016) for $A-A'$ and $E-E'$, respectively (figs. 7 and 8). We then modified these models using mapped geologic relations and density information. The amplitude of the anomaly is not the only attribute to match; matching its gradients provides important information on source depth and shape.

We chose profile $E-E'$ (fig. 8) to be co-located with that of Abdelwahed and others (2016), as the tomography model was not available digitally. The cross section through the tomographic model is shown as velocity perturbations from the average velocity (fig. 8C). We drew bodies in figure 8D based on the velocity contours in figure 8C, averaged the velocities in each body, and then converted the velocity contrast, assuming the reference velocity to be 6.2 km/s, to density contrast using the linear relation for all rocks (except monomineralic and volcanic rocks) of Christensen and Mooney (1995); note that the same density contrasts resulted from a reference velocity of 6.6 km/s. We chose profile $A-A'$ (fig. 7) to be co-located with the shear-wave velocity profile of Civilini (2018), derived from ambient-noise sources using radial-radial (outward) phase velocities (his figure 4.21). We drew bodies of average shear-wave velocity from his profile figure, converted shear-wave velocity to P-wave velocity using a factor of 1.67 (Stein and Wysession, 2003), and then converted to density using the Christensen and Mooney (1995) relation. The forward gravity models are both referenced to values over basement outcrops at the western ends of the profiles.

Predicted gravity curves from the P-wave and shear-wave velocity models do not fit the observed gravity well. This is not surprising, given that resolution tests for the P-wave tomography and the shear-wave velocity models indicate that features smaller than 7 km and 30 km, respectively, may not be resolved (Abdelwahed and others, 2016; Civilini, 2018). For profile $A-A'$, the shear-wave velocity model does not predict the breadth or magnitude of the observed gravity low over Harrat Rahat and greatly underestimates the mass on the eastern end of the profile (thick, solid blue line labeled “calculated total crust” in fig. 7). The predicted gravity high over eastern Harrat Rahat (thick, solid blue line in fig. 7) results from faster shear-wave velocities in the upper 20 km (orange line labeled “calculated upper crust only” in fig. 7); the slower velocities below 20 km do not offset the

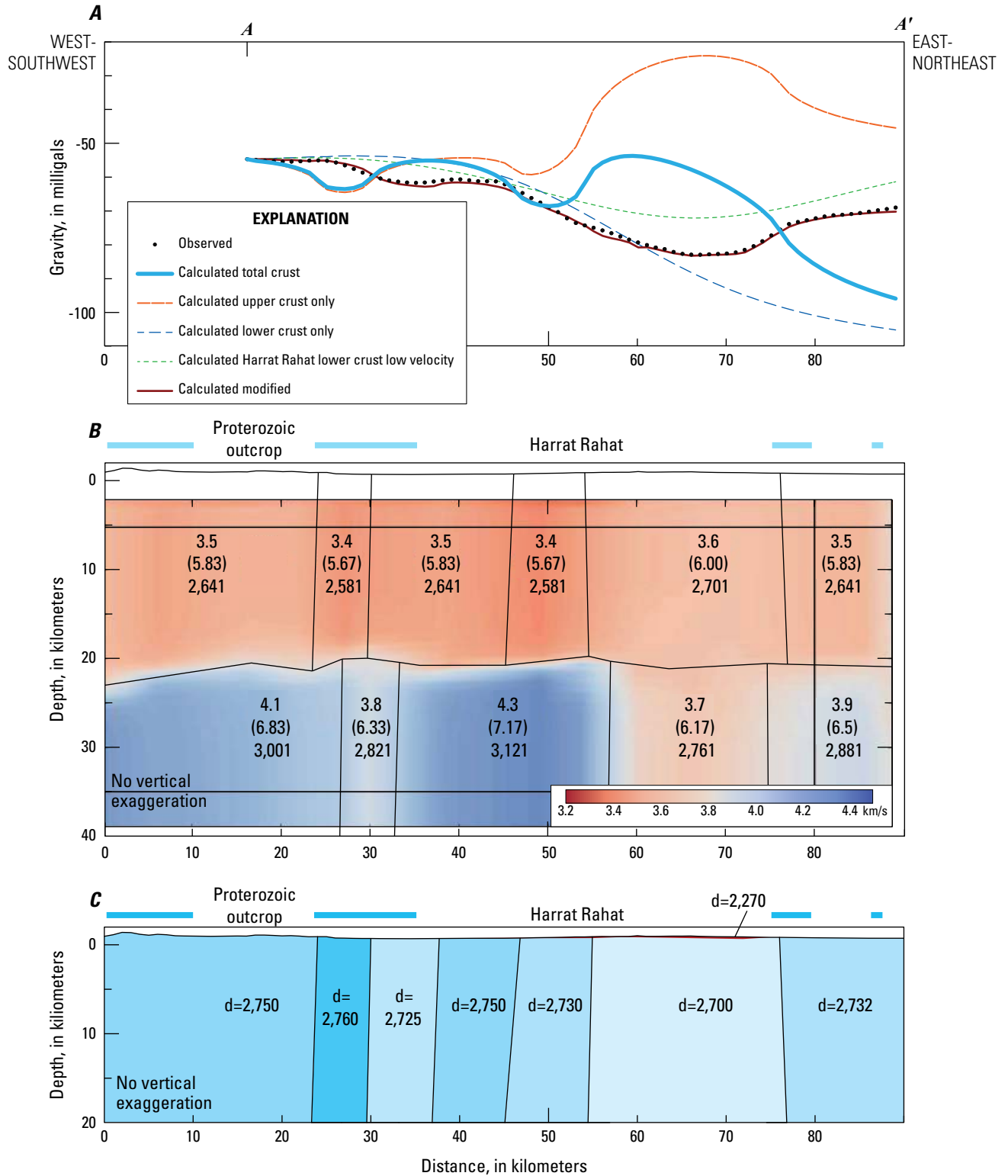


Figure 7. Forward gravity models of profile A–A'. *A*, Observed gravity values (from grid) and predicted gravity variations from densities derived from shear-wave velocity (see text). *B*, Shear-wave velocity profile of Civilini (2018). Numbers in blocks refer to shear-wave velocity in kilometers per second (km/s) (top number), compressional-wave velocity in km/s (middle number), and density in kilograms per cubic meter (kg/m³) (bottom number). *C*, Modified density distribution limited to the upper 20 kilometers (see text). Numbers are density in kg/m³. Gravity effect of this crustal density distribution produces the curve labeled “calculated modified” in *A*.

12 Active Volcanism on the Arabian Shield—Geology, Volcanology, and Geophysics

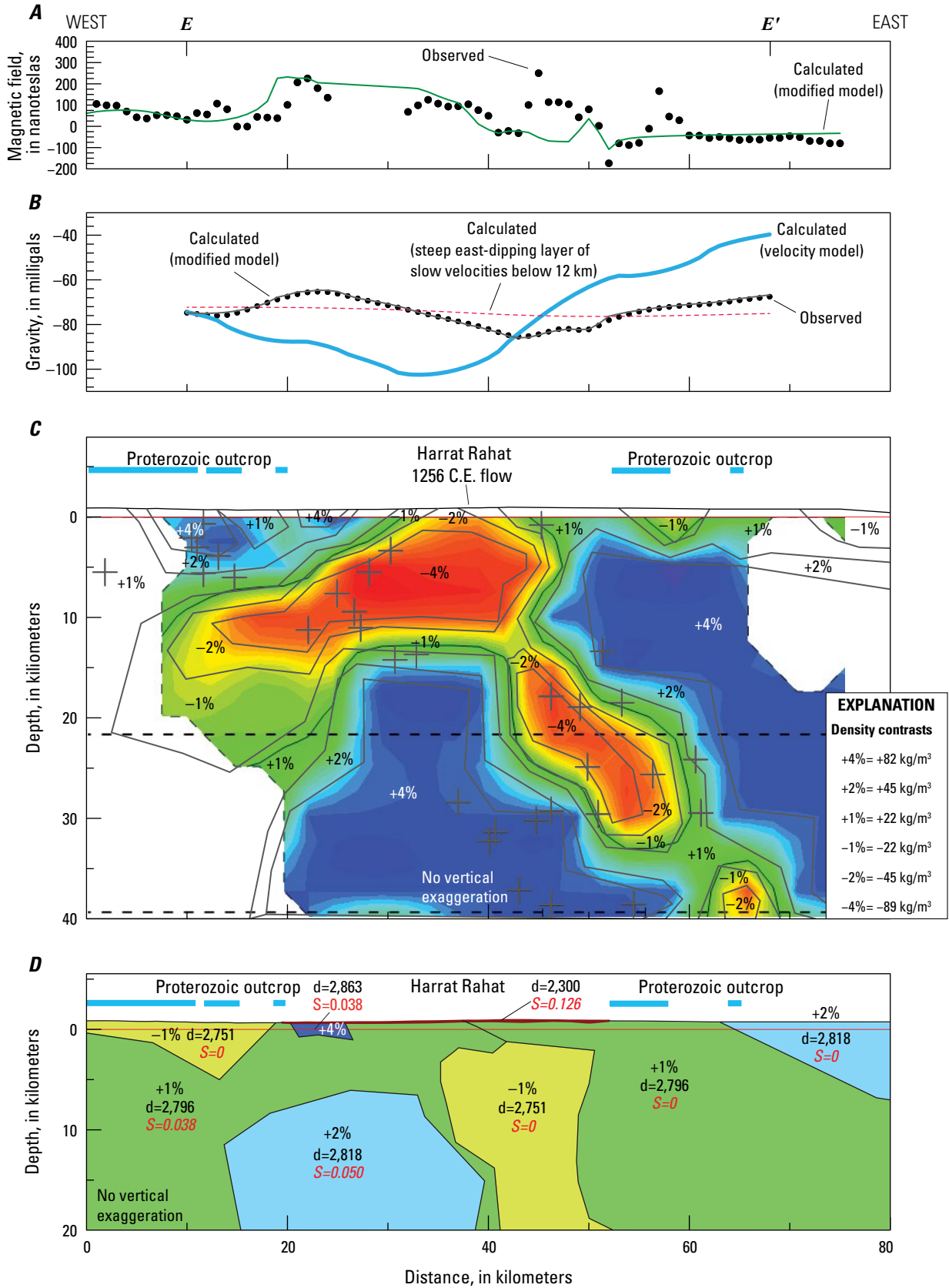


Figure 8 (page 12). Forward gravity models of profile $E-E'$. *A*, Observed magnetic values from grid and predicted magnetic variations from the distribution of magnetic susceptibility in *D*. *B*, Observed gravity values from grid and predicted gravity variations from densities derived from tomographic P-wave velocity model (*C*) and modified model (*D*). *C*, Background from figure 6 of Abdelwahed and others (2016), which shows P-wave velocity perturbations from the average velocity. Numbers in *C* refer to P-wave velocity perturbations averaged within each polygon defined by gray lines. Crosses denote located earthquakes (see Abdelwahed and others, 2016). *D*, Modified density distribution for the upper 20 kilometers of crust (see text). The three numbers in each polygon represent, from top to bottom, the velocity perturbation in percent (%); rock density, d , in kilograms per cubic meter (kg/m^3); and magnetic susceptibility, S , in 10^{-3} SI units.

upper crustal contribution. Although part of the amplitude of the gravity low can be fit assuming the upper crust is homogeneous and the slow velocity area beneath the volcanic field is the only heterogeneity in the lower crust (otherwise set to shear-wave velocity of 4.1 km/s; green dashed line in fig. 7), the predicted gradients are too gentle and do not match those observed along the profile. For profile $E-E'$ (fig. 8), predicted gravity greatly overestimates mass on its eastern end and the predicted gravity low is offset 10–15 km west of the observed gravity low. Although the tomography model indicates slow velocities at depths ≥ 12 km directly beneath the gravity low, the density contrast and its depth produce a 4-mGal low spread over a distance of more than 40 km.

The forward models based on seismic velocity data suggest that the gravity low is mostly sourced within the upper to middle crust (about 20 km). Although lower crustal sources contribute to the low, the anomalies they produce are too broad to be addressed with the distribution of gravity measurements. Thus, we modified these models to restrict density variations to the upper 20 km (bottom panels in figs. 7 and 8). At about this depth, seismic refraction data across the Arabian Shield (Mooney and others, 1985) and shear-wave velocity models (Tang and others, 2016; Civilini, 2018) indicate a discontinuity that separates the upper from the lower crust. The observed gravity variations along profile $A-A'$ can be fit by the volcanic cover and lower density basement material beneath Harrat Rahat; the modeled basement density variations are well within those measured on basement samples (fig. 5). One can fit the observed gravity variations by restricting density variations to the upper 10 km with larger density contrasts. The observed gravity variations along profile $E-E'$ can be fit by shifting the slow velocities in the upper 10 km of crust approximately 10 km east beneath the axis of Harrat Rahat. The predicted density variations are again well within the observed range of measured densities on basement samples. We also show magnetic anomalies along this profile that indicate higher magnetic values west of Harrat Rahat than to the east; this first-order difference can be fit by magnetic crust west of Harrat Rahat and west of the 1256 C.E. volcanic vents.

Discussion

The gravity low along the main vent axis of Harrat Rahat must be caused by both the volcanic field and the underlying basement, as indicated by the northward extension of the gravity low onto basement outcrops. With gravity data alone, we cannot determine if basement density variations predate or are caused by Cenozoic volcanism and intrusion. However,

the rough coincidence of basement gravity variations (fig. 6A) with spatial density variations measured on Proterozoic basement samples (fig. 5A) indicates that at least part of the gravity low is caused by Proterozoic basement. For example, the decrease in basement gravity values along the east side of Harrat Rahat is mirrored by basement density measurements. The lowest densities measured on basement samples coincide with low basement gravity values north of Harrat Rahat. A prominent north-trending basement syncline coincides with the lowest gravity values (fig. 2); the continuation of the gravity low to the south may argue for continuation of this Proterozoic structure. Although the basement gravity low can be easily produced solely from Proterozoic density variations, as modeled in profiles $A-A'$ and $E-E'$, it cannot be solely the result of partial melt and increased temperatures. Assuming a coefficient of thermal expansion of $2 \times 10^{-15} \text{ } ^\circ\text{C}^{-1}$ (Richter and Simmons, 1974), the modeled density contrasts lead to temperature differences of 600–1,200 $^\circ\text{C}$ from the surface to 20 km depth, which is clearly unreasonable. However, the gravity models do not rule out small volumes of partial melt and increased temperatures beneath Harrat Rahat at depth, as these would produce broad, low-amplitude anomalies that cannot be fully modeled or resolved with the spatial extent of our gravity measurements. Higher V_p/V_s (ratio of P-wave to S-wave velocity) values at seismic station RH01 (fig. 2) relative to surrounding seismic stations can be explained by crust that is on average more mafic than that to the west, east, or south; alternatively, higher V_p/V_s values can result from partial melt. Station RH01 lies within the basement gravity low, which would argue against more mafic crust. Alternatively, fluids and fracturing can explain higher V_p/V_s ratios as well as explain the mismatch between the predicted gravity anomalies from the seismic velocity profiles and the observed gravity anomalies. Although Aboud and others (2018) interpreted conductive anomalies in the middle crust as resulting from partial melt, only a handful of their soundings were on Proterozoic basement, limited along the eastern margin of the harrat, and thus make it more difficult to assess other sources such as anisotropy within the basement. An integrated approach using all the various geophysical techniques would be useful to differentiate between these various sources.

The volcanic basin thickness model from the inversion of the gravity data (fig. 6A) reveals thicker volcanic rocks roughly along the main vent axis. The inversion assumes no lateral variations in the volcanic fill. Given the spatial variations of density measurements of volcanic rocks (fig. 5A), the volcanic fill may be underestimated in the western part of

Harrat Rahat and overestimated beneath the trachyte domes, which would result in a more uniform thickness across the harrat. This method cannot distinguish volcanic deposits from underlying Cenozoic sedimentary deposits, so our estimate of total volcanic basin volume (460 km^3) may be considered a maximum estimate of the volume of volcanic flows emanating from this part of Harrat Rahat. Well information on depth to basement would provide an extremely valuable constraint for improving the basin model.

For all its caveats, the volcanic basin model (fig. 6A) compares favorably with those of Blank and Sadek (1983; based on spectral analysis of aeromagnetic flightline data) and Daesslé and Durozoy (1972; based on “geophysics”) in that the thickest part of the fill trends parallel to the vent axis of Harrat Rahat and is only about 100–200 m greater than their maximum thickness results. Our basin model differs significantly from that of Aboud and others (2015; based on Euler deconvolution of aeromagnetic gridded data), which predicts 1–2 km of basin fill interpreted as a graben. However, the thickest parts of their model are restricted to the area with lower resolution aeromagnetic data. Thus, short-wavelength magnetic anomalies caused by near-surface volcanic rocks are severely undersampled and aliased, and this introduction of long-wavelength artifacts may have caused overestimation of Euler-determined depths to basement. Furthermore, their results predict basin fill more than 600 m thick over areas of basement outcrop; see figure 9 for a comparison of basement surfaces derived here and from Aboud and others (2015) along their model profiles. The basement surface derived from poorly sampled magnetic data cannot explain the observed gravity in a geologically reasonable way. Although Aboud and others (2018) assert that their magnetotelluric results are consistent with a graben structure defined by gravity presented by Aboud

and others (2015), the two model profiles shown by Aboud and others (2015) use the inversion of magnetic data to provide the depth to basement; two very different density contrasts are used in these models and are not documented or discussed in their paper. Furthermore, results from a more comprehensive magnetotelluric study (Bedrosian and others, 2019) are consistent with the depth to basement derived in this study.

Our model does not reveal a prominent graben bounded by large-offset normal faults, but rather a broad depression of the basement surface that is deeper along the eastern part of the harrat and in the southwest part of the volcanic field (fig. 10). Extension that produced the depression appears to have been accommodated by distributed, small-offset faults. The age of the depression must postdate Miocene basalt flows that are perched 300–400 m above Harrat Rahat west of Al Madīnah (Pellaton, 1981); these flows have been dated by the $^{40}\text{Ar}/^{39}\text{Ar}$ method at 13.0 to 14.2 Ma (Calvert and Sisson, 2023; formerly dated by K/Ar method at 11–8 Ma by Pellaton, 1981). Cooling and denudation, a proxy for extension, began at 25–20 Ma in southern Arabia (Bohannon and others, 1989) and accelerated after ~14 Ma; modeling of longitudinal river profiles that drain Harrat Rahat indicate that uplift also started at about 30–20 Ma and peaked at ~15 Ma (Wilson and others, 2014). Therefore, most of the subsidence that formed the basin beneath Harrat Rahat likely formed during the middle to late Miocene, soon after eruption of the perched basalts.

Both of the basement downwarps beneath the harrat trend parallel to the main vent axis and the secondary vent axis to the west, as well as to gravity and magnetic gradients south from Al Madīnah to the latitude of Um Rgaibah, which lies on a basement high. South of Um Rgaibah, the topographic axis of Harrat Rahat shifts 5–10 km to the southwest, as does

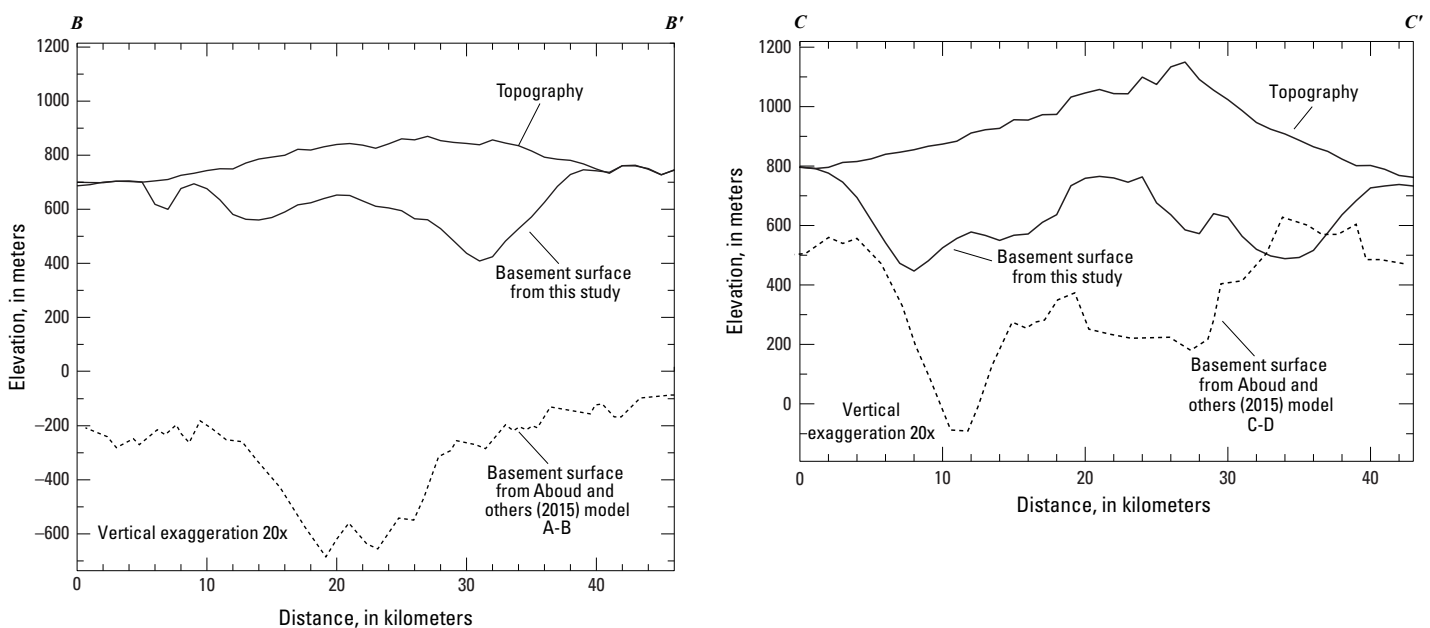


Figure 9. Plot of topography and basement surfaces across Harrat Rahat. Left panel, profile *B–B'*. Right panel, profile *C–C'*. Location of profiles shown in figure 2. Vertical exaggeration 20:1.

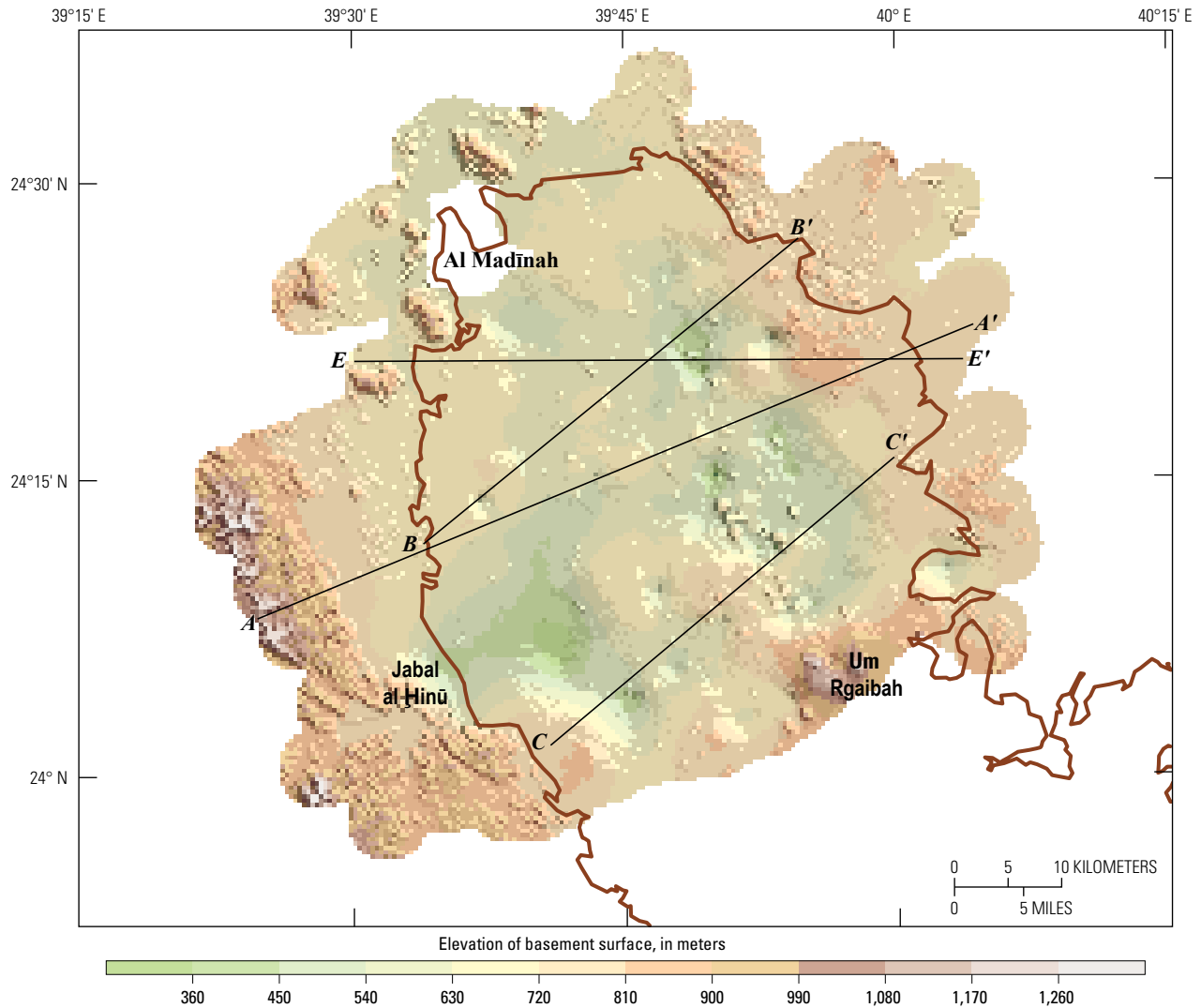


Figure 10. Map of the elevation of basement surface. Black lines, modeled cross sections. Brown line, outline of Harrat Rahat volcanic field.

the next trachyte center to the south. The southwest margin of the basement high at Um Rgaibah is parallel to the Najd Fault System, perhaps suggesting influence of older Proterozoic structure on pathways of magma to the vent axis.

Conclusions

We use gravity data for the first time to reveal the basin configuration beneath northern Harrat Rahat and also density variations within the underlying basement. A prominent gravity low that coincides with the main vent axis results from thicker volcanic fill and less dense basement. The secondary vent axis coincides with the western margin of the gravity low. Low densities within the basement most likely are caused by lithologic variations in the basement, thus predating effects

of Cenozoic volcanism. The gravity data do not rule out modification of basement rocks by small volumes of partial melt and higher temperatures or extensive fracturing and fluids at depth.

Acknowledgments

Drew Downs, David Sherrod, Andrew Calvert, Thomas Sisson, Mark Stelten, Hannah Dieterich, and Juliet Ryan-Davis provided us with rock samples for physical property measurements. Richard Blakely and Paul Bedrosian provided helpful comments that improved the paper. We also thank Mark Gettings of the U.S. Geological Survey and two anonymous reviewers. This study was funded by the Saudi Geological Survey.

References Cited

- Abdelwahed, M.F., El-Masry, N., Moufti, M.R., Kenedi, C.L., Zhao, D., Zahran, H., and Shawali, J., 2016, Imaging of magma intrusions beneath Harrat Al-Madinah, in Saudi Arabia: *Journal of Asian Earth Sciences*, v. 120, p. 17–28.
- About, E., El-Masry N., Qaddah, A., Alqahtani, F., and Moufti, M.R.H., 2015, Magnetic and gravity data analysis of Rahat volcanic field, El-Madinah city, Saudi Arabia: *NRIAG Journal of Astronomy and Geophysics*, v. 4, p. 154–162.
- About, E., Wameyo, P., Alqahtani, F., and Moufti, M.R., 2018, Imaging subsurface northern Rahat volcanic field, Madinah city, Saudi Arabia, using magnetotelluric study: *Journal of Applied Geophysics*, v. 159, p. 564–572.
- Baranov, V.I., 1957, A new method for interpretation of aeromagnetic maps—Pseudogravimetric anomalies: *Geophysics*, v. 22, p. 359–383.
- Bedrosian, P.A., Peacock, J.R., Dhary, M., Sharif, A., Feucht, D.W., and Zahran, H., 2019, Crustal magmatism and anisotropy beneath the Arabian Shield—A cautionary tale: *Journal of Geophysical Research*, v. 124, p. 10153–10179, <https://doi.org/10.1029/2019JB017903>.
- Blakely, R.J., and Simpson, R.W., 1986, Approximating edges of source bodies from magnetic or gravity anomalies: *Geophysics*, v. 51, p. 1494–1498.
- Blank, H.R., 1977, Aeromagnetic and geologic study of Tertiary dikes and related structures on the Arabian margin of the Red Sea in Red Sea Research 1970–1975: Saudi Arabian Directorate General of Mineral Resources Bulletin 22, p. G1–G18.
- Blank, H.R., and Sadek, H.S., 1983, Spectral analysis of the 1976 aeromagnetic survey of Harrat Rahat, Kingdom of Saudi Arabia: U.S. Geological Survey Open-File Report 83–640, 29 p., 2 plates.
- Bohannon, R.G., Naeser, C.W., Schmidt, D.L., and Zimmermann, R.A., 1989, The timing of uplift, volcanism, and rifting peripheral to the Red Sea—A case for passive rifting: *Journal of Geophysical Research*, v. 94, p. 1683–1701.
- Briggs, I.C., 1974, Machine contouring using minimum curvature: *Geophysics*, v. 39, p. 39–48.
- Brocher, T.M., 2005, Compressional and shear wave velocity versus depth in the San Francisco Bay Area, California—Rules for USGS Bay Area Velocity Model 05.0.0: U.S. Geological Survey Open-File Report 05–1317, 58 p.
- Calvert, A.T., and Sisson, T.W., 2023, Cenozoic tectonics of the western Arabia Plate related to harrat magmatism near Al Madīnah, Kingdom of Saudi Arabia, chap. B of Sisson, T.W., Calvert, A.T., and Mooney, W.D., eds., *Active volcanism on the Arabian Shield—Geology, volcanology, and geophysics of northern Harrat Rahat and vicinity, Kingdom of Saudi Arabia*: U.S. Geological Survey Professional Paper 1862 [also released as Saudi Geological Survey Special Report SGS–SP–2021–1], 28 p., <https://doi.org/10.3133/pp1862B>.
- Camp, V.E., 1986, Geologic map of the Umm al Birak quadrangle, sheet 23D, Kingdom of Saudi Arabia (with text): Saudi Arabian Directorate General of Mineral Resources Geologic Map GM-87C, scale 1:250,000, 40 p.
- Camp, V.E., Hooper, P.R., Roobol, M.J., and White, D.L., 1987, The Madinah eruption, Saudi Arabia—Magma mixing and simultaneous extrusion of three basaltic chemical types: *Bulletin of Volcanology*, v. 49, p. 489–508.
- Camp, V.E., and Roobol, J.M., 1989, The Arabian continental alkali basalt province; Part I—Evolution of Harrat Rahat, Kingdom of Arabia: *Geological Society of America Bulletin*, v. 101, p. 71–95.
- Camp, V.E., and Roobol, J.M., 1992, Upwelling asthenosphere beneath western Arabia and its regional implications: *Journal of Geophysical Research*, v. 97, p. 15255–15271.
- Christensen, N.I., and Mooney, W.D., 1995, Seismic velocity structure and composition of the continental crust—A global view: *Journal of Geophysical Research*, v. 100, p. 9761–9788.
- Civilini, F., 2018, Determining seismic shear-velocity from ambient noise sources at regional and local scales: Wellington, New Zealand, Victoria University of Wellington, Ph.D. dissertation, 313 p.
- Coleman, R.G., 1993, Geologic evolution of the Red Sea: *Oxford Monographs on Geology and Geophysics*, v. 34, 186 p.
- Coleman, R.G., Gregory, R.T., and Brown, G.F., 1983, Cenozoic volcanic rocks of Saudi Arabia: U.S. Geological Survey Open-File Report 83–788, 82 p., 1 plate.
- Cordell, L., and Grauch, V.J.S., 1985, Mapping basement magnetization zones from aeromagnetic data in the San Juan Basin, New Mexico in Hinze, W.J., ed., *The utility of regional gravity and magnetic anomaly maps*: Tulsa, Okla., Society of Exploration Geophysicists, p. 181–197.
- Daesslé, M., and Durozoy, G., 1972, Jabal Sayid water supply, the Harrat Rahat basalt: French Bureau de Recherches Géologiques et Minières Technical Record 72-JED-2, 21 p., 1 app., 1 sheet, 1 cross section.

- Dietterich, H.R., Stelten, M.E., Downs, D.T., and Champion, D.E., 2017, Spatial and temporal analysis of eruption locations, compositions, and styles in northern Harrat Rahat, Kingdom of Saudi Arabia [abs.]: American Geophysical Union, 2017 Fall Meeting, abstract V51B-0352.
- Downs, D.T., Robinson, J.E., Stelten, M.E., Champion, D.E., Dietterich, H.R., Sisson, T.W., Zahran, H., Hassan, K., and Shawali, J., 2019, Geologic map of the northern Harrat Rahat volcanic field, Kingdom of Saudi Arabia: U.S. Geological Survey Scientific Investigations Map 3428 [also released as Saudi Geological Survey Special Report SGS-SP-2019-2], 65 p., 4 sheets, scales 1:75,000, 1:25,000, <https://doi.org/10.3133/sim3428>.
- Downs, D.T., Stelten, M.E., Champion, D.E., Dietterich, H.R., Nawab, Z., Zahran, H., Hassan, K., and Shawali, J., 2018, Volcanic history of the northernmost part of the Harrat Rahat volcanic field, Saudi Arabia: *Geosphere*, v. 14, no. 3, p. 1253–1282.
- Hansen, S., Schwartz, S., Al-Amni, A., and Rodgers, A., 2006, Combined plate motion and density-driven flow in the asthenosphere beneath Saudi Arabia—Evidence from shear-wave splitting and seismic anisotropy: *Geology*, v. 34, p. 869–872.
- Jachens, R.C., and Moring, B.C., 1990, Maps of the thickness of Cenozoic deposits and the isostatic residual gravity over basement for Nevada: U.S. Geological Survey Open-File Report 90–404, 15 p., 2 plates.
- Kauahikaua, J., Hildenbrand, T., and Webring, M., 2000, Deep magmatic structures of Hawaiian volcanoes, imaged by three-dimensional gravity models: *Geology*, v. 28, p. 883–886.
- Langenheim, V.E., 2018, Gravity and physical property data of the northern Harrat Rahat, Saudi Arabia: U.S. Geological Survey data release, accessed October 31, 2018, at <https://doi.org/10.5066/P9THCSE8>.
- Langenheim, V.E., Ritzinger, B.R., Zahran, H., Shareef, A., and Al-dahri, M., 2019, Crustal structure of the northern Harrat Rahat volcanic field (Saudi Arabia) from gravity and aeromagnetic data: *Tectonophysics*, v. 750, p. 9–21.
- Levin, V., and Park, J., 2000, Shear zones in the Proterozoic lithosphere of the Arabian Shield and the nature of the Hales discontinuity: *Tectonophysics*, v. 323, p. 131–148.
- Loni, O.A., 2005, Geophysical characteristics of the subsurface structures in northeastern Al-Madinah Al-Munawarah (Harrat Al-Aqul) Central Arabian shield: Riyadh, Saudi Arabia, King Saud University, M.S. thesis, 257 p.
- Mooney, W.D., Gettings, M.E., Blank, H.R., and Healy, J.H., 1985, Saudi Arabian seismic-refraction profile—A traveltime interpretation of crustal and upper mantle structure: *Tectonophysics*, v. 111, p. 173–246.
- Moufti, M.R., Moghazi, A.M., and Ali, K.A., 2013, ⁴⁰Ar/³⁹Ar geochronology of the Neogene-Quaternary Harrat Al-Madinah intercontinental volcanic field, Saudi Arabia—Implications for duration and migration of volcanic activity: *Journal of Asian Earth Sciences*, v. 62, p. 253–268.
- Pallister, J.S., McCausland, W.A., Jónsson, S., Lu, Zhong, Zahran, H.M., El Hadidy, S., Aburukbah, A., Stewart, I.C., Lundgren, P.R., White, R.A., and Moufti, M.R.H., 2010, Broad accommodation of a rift-related extension recorded by dyke intrusion in Saudi Arabia: *Nature Geoscience*, v. 3, p. 705–712.
- Pellaton, C., 1981, Geologic map of the Al Madinah quadrangle, sheet 24D, Kingdom of Saudi Arabia (with text): Saudi Arabian Directorate General of Mineral Resources Geologic Map GM-52C, scale 1:250,000, 19 p.
- Phillips, J.D., 2001, Designing matched bandpass and azimuthal filters for the separation of potential-field anomalies by source region and source type: Australian Society of Exploration Geophysicists, 15th Geophysical Conference and Exhibition, Expanded Abstracts CD-ROM, 4 p.
- Reid, A.B., 1980, Aeromagnetic survey design: *Geophysics*, v. 45, p. 973–976.
- Richter, D., and Simmons, G., 1974, Thermal expansion behavior of igneous rocks [abs.]: *International Journal of Rock Mechanics and Mining Sciences and Geomechanics Abstracts*, v. 11, no. 10, p. 403–411.
- Robinson, J.E., and Downs, D.T., 2023, Overview of the Cenozoic geology of the northern Harrat Rahat volcanic field, Kingdom of Saudi Arabia, chap. R of Sisson, T.W., Calvert, A.T., and Mooney, W.D., eds., *Active volcanism on the Arabian Shield—Geology, volcanology, and geophysics of northern Harrat Rahat and vicinity*, Kingdom of Saudi Arabia: U.S. Geological Survey Professional Paper 1862 [also released as Saudi Geological Survey Special Report SGS-SP-2021-1], 20 p., scale 1:100,000, <https://doi.org/10.3133/pp1862R>.
- Rodgers, A.J., Walter, W.R., Mellors, R.J., Al-Amri, A.M.S., and Zhang, Y-S., 1999, Lithospheric structure of the Arabian Shield and Platform from complete regional waveform modeling and surface wave group velocities: *Geophysical Journal International*, v. 138, p. 871–878.
- Runge, M.G., Bebbington, M.S., Cronin, S.J., Lindsay, J.M., and Moufti, M.R., 2016, Integrating geological and geophysical data to improve probabilistic hazard forecasting of Arabian Shield volcanism: *Journal of Volcanology and Geothermal Research*, v. 311, p. 41–59.

- Stein, S., and Wysession, M., 2003, Introduction to seismology, earthquakes, and Earth structure: Blackwell Publishing, Malden, Mass., 1,261 p.
- Stelten, M.E., Downs, D.T., Champion, D.E., Dieterich, H.R., Calvert, A.T., Sisson, T.W., Mahood, G.A., and Zahran, H.M., 2023, Eruptive history of northern Harrat Rahat—Volume, timing, and composition of volcanism over the past 1.2 million years, chap. D of Sisson, T.W., Calvert, A.T., and Mooney, W.D., eds., Active volcanism on the Arabian Shield—Geology, volcanology, and geophysics of northern Harrat Rahat and vicinity, Kingdom of Saudi Arabia: U.S. Geological Survey Professional Paper 1862 [also released as Saudi Geological Survey Special Report SGS-SP-2021-1], 46 p., <https://doi.org/10.3133/pp1862D>.
- Stelten, M.E., Downs, D.T., Dieterich, H.R., Mahood, G.A., Calvert, A.T., Sisson, T.W., Zahran, H., and Shawali, J., 2018, Timescales of magmatic differentiation from alkali basalt to trachyte within the Harrat Rahat volcanic field, Kingdom of Saudi Arabia: Contributions to Mineralogy and Petrology, v. 173, no. 68, 17 p., <https://doi.org/10.1007/s00410-018-1495-9>.
- Stern, R.J., and Johnson, P., 2010, Continental lithosphere of the Arabian Plate—A geologic, petrologic, and geophysical synthesis: Earth-Science Reviews, v. 101, p. 29–67.
- Tang, Z., Julia, J., Zahran, Z., and Mai, P.M., 2016, The lithospheric shear-wave velocity structure of Saudi Arabia—Young volcanism in an old shield: Tectonophysics, v. 680, p. 8–27.
- Webring, M., 1981, MINC—A gridding program based on minimum curvature: U.S. Geological Survey Open-File Report 81-1224, 41 p.
- Wilson, J.W.P., Roberts, G.G., Hoggard, M.J., and White, N.J., 2014, Cenozoic epeirogeny of the Arabian Peninsula from drainage modeling: Geochemistry, Geophysics, Geosystems, v. 15, p. 3723–3761.
- Zahran, H., Stewart, I.C.F., Johnson, P.R., and Basahel, M.H., 2003, Aeromagnetic-anomaly maps of central and western Saudi Arabia: Saudi Geological Survey Open-File Report SGS-OF-2002-8, 6 p., 4 plates.

Moffett Field Publishing Service Center, California
Manuscript approved October 15, 2019
Edited by Claire Landowski
Layout and design by Kimber Petersen
Illustration support by Katie Sullivan

